Capability Analysis for an Inductively Coupled Power Transfer System

John I. Rodriguez Deron K. Jackson Steven B. Leeb

Abstract—

This paper reviews a computer-aided analytical technique for predicting the power transfer capability of an AC inverter energizing a separable inductive coupling. The capability curve is obtained using a switching model of the output rectifier and a readily available software package such as MATLAB®. The capability curve is useful, among other applications, for evaluating candidate separable transformer designs. Conceptually, it can be used to analyze any transformer-isolated, DC-DC power conversion stage.

I. Background

For servomechanical applications, including battery charging, we are exploring a two-stage DC-DC converter architecture that uses a separable transformer for connecting a load to the utility [1] – [8]. The first stage, a power factor correcting (PFC) utility interface, provides a pre-regulated DC voltage to the second power stage, a symmetric half-bridge DC-DC converter capable of bidirectional power flow. The half-bridge converter serves as an isolation stage, transfering power from the PFC output across the inductively coupled connector. First, a high frequency AC inverter converts the PFC bus voltage into a square wave suitable for energizing the primary winding. On the secondary side, the induced AC voltage is then rectified and delivered to the load.

Control of the load voltage is achieved by varying the PFC output voltage that supplies the high-frequency inverter. This control scheme allows the inverter to be operated at a fixed frequency and unity duty ratio, a mode of operation which is attractive for two reasons [9]. First, a fixed frequency allows for further optimization of the magnetic components in the inductive coupling. Second, a unity duty ratio results in rectifier side AC voltage components that are small enough to be supported by the transformer leakage inductance, thus eliminating the need for an output inductor. As an added benefit, the leakage inductance also facilitates zero-voltage switching (ZVS) of the inverter.

Figure 1 is a model of the symmetric half-bridge converter and the inductive coupling (represented here with a "T" transformer model). Ideally the DC-DC stage would function as a perfect transformer, delivering a DC output voltage scaled by the transformer turns ratio, N_s/N_p. Unfortunately, the leakage inductance also limits the power transfer capability of the DC-DC stage. These power limits

John I. Rodriguez and Steven B. Leeb are with the Laboratory for Electromagnetic and Electronic Systems, Massachusetts Institute of Technology, Cambridge, MA 02139, USA. Deron K. Jackson is a Senior Hardware Engineer at Adept Technology, San Jose, CA 95134, USA.

0-7803-6561-5/00/$10.00 © 2000 IEEE

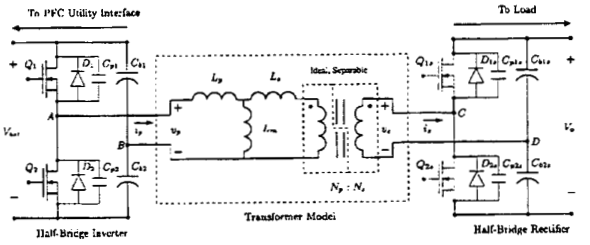

Fig. 1. Symmetric Half-bridge DC-DC converter.

are exacerbated in the case of a transformer that is separable, because mechanical separability can impose a higher leakage-to-magnetizing inductance ratio than might otherwise be achieved. For a given servomechanical application, it is essential to know if a converter design is capable of providing the required power at a specified output voltage. This paper reviews a computer-aided analytical technique for determining the power transfer capability of DC-DC power stages employing a transformer.

II. Transfer Characteristic

The term "DC transfer characteristic" describes how a converter's input-to-output voltage ratio varies as a function of the load. The problem of determining power transfer capability arises in many engineering problems, for example, the analysis of transmission lines. A recent example of the application of impedance analysis and shaping to optimize power transfer in a power electronic system is presented in [10]. Because a finite leakage inductance is present, the DC-DC converters analyzed in this paper exhibit load regulation, i.e. an output voltage that droops with increasing load power. In essence, the leakage inductance and load effectively form a voltage divider. This phenomenon can significantly limit the deliverable load power if the leakage inductance is too large. Therefore, it is important to have a computer-aided tool to predict the droop and to assist in system design. In particular, the ability to quickly analyze power delivery capability of the overall DC-DC stage permits quick evaluation of candidate separable transformer designs, and avoids the need for computationally intensive, cycle by cycle simulations of the converter.

Two approaches, well-suited to analytical software packages such as MATLAB® are presented for comparison: a "classic" reactance model similar to those seen in the context of line-frequency rectifiers, and a more refined switching model that focuses on the specific waveform behavior of the rectifier. For simplicity, we show a resistive load in

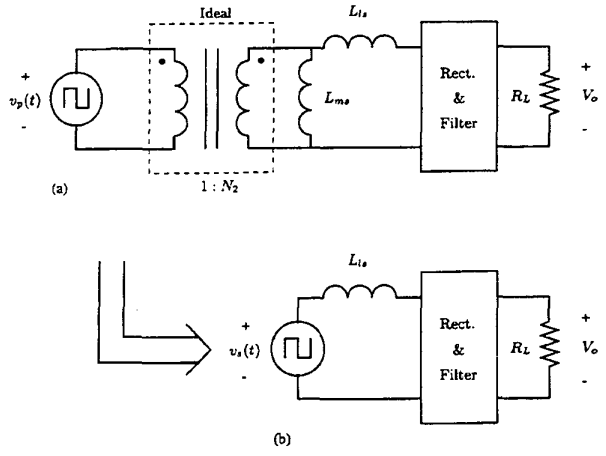

Fig. 2. Half-bridge inverer and transformer simplifications.

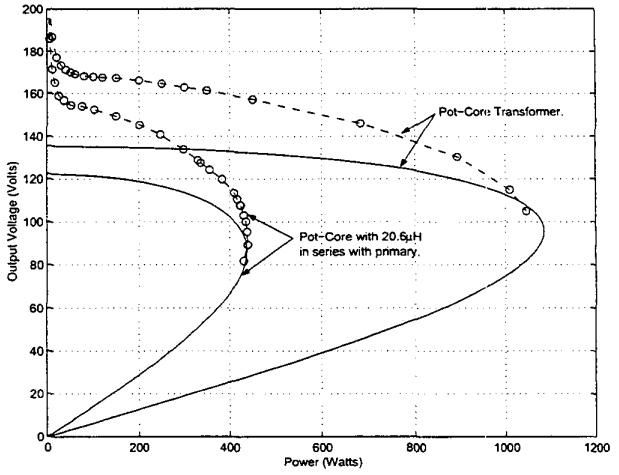

Fig. 3. Capability Curve prediction using the reactance model.

the work which follows. However these analyses are developed without assuming a specific load model. Hence, these capability curves are applicable to any load that can settle to a steady-state DC operating point.

Figure 2(a) shows a simplified model of the DC-DC converter. The primary-side inverter has been replaced by an equivalent square-wave voltage source,

$$v_p(t) = \frac{V_{bst}}{2} sgn[sin(2\pi f_s t)], \tag{1}$$

where V_{bst} is the DC bus voltage supplied by the UPC boost pre-regulator and f_s is the switching frequency of the half-bridge inverter. In addition, the inductive coupling previously modeled as "T" network has been converted into an electrically equivalent "L" model with secondary-side inductances. Because the magnetizing inductance L_{ms} cannot influence the output in this model, only the leakage inductance L_{ls} and effective turns ratio N_2 are determined:

$$L_{ls} = \left(\frac{N_s}{N_p}\right)^2 \left(L_s + \frac{L_p L_m}{L_m + L_p}\right), \tag{2}$$

$$N_2 = \left(\frac{N_s}{N_p}\right) \left(\frac{L_m}{L_m + L_p}\right). \tag{3}$$

As a final reduction, Figure 2(b) shows the network after reflecting the primary-side source across the transformer, all that remains is the newly defined secondary-side source, $v_s(t)$ driving the rectifier block through the leakage inductance L_{ls}, where

$$v_s(t) = V_s sgn[sin(2\pi f_s t)], \quad V_s = \frac{N_2 V_{bst}}{2}. \tag{4}$$

These initial simplifications are common to both analyses and provide a convenient starting point.

III. Reactance Model

A reactance model is developed by replacing the square-wave $v_s(t)$, with its sinewave fundamental:

$$v_{s_1}(t) = V_{s_1} sin(2\pi f_s t), \quad V_{s_1} = \frac{4V_s}{\pi}. \tag{5}$$

This derivation assumes steady state operation and an excitation frequency high enough to insure that the output voltage remains constant over each switching period. For simplicity the rectifier diodes are also treated as ideal and their parasitic capacitances ignored. Under these assumptions it can been shown that the average output voltage, V_o, is a function of the "effective" reactance X_c and load R_L as follows:

$$V_o = \frac{4V_{s_1}}{\pi} \frac{R_L}{\sqrt{(X_c)^2 + R_L^2}}, \quad X_c = 8\pi L_{ls} f_s \tag{6}$$

Equation (6) clearly illustrates the impact of the leakage inductance on the output voltage, taking a form similar to what one would encounter when determining the magnitude of a sinusoidal steady state voltage across a resistive load in an L-R network. By substituting $R_L = V_o^2/P_o$ into (6), an equation relating output power to output voltage can be found:

$$P_o = \frac{V_o \sqrt{(4V_{s_1}/\pi)^2 - V_o^2)}}{X_c}. \tag{7}$$

Predicted and measured capability curves are shown in Fig. 3 for a 1500 watt prototype converter. Two pairs of predicted and experimental curves are presented. One pair of curves corresponds to a pot-core transformer. For the second pair an additional 20.6μH inductor was added in series with the transformer primary in order to approximate a larger leakage inductance. Both experimental curves were measured with $V_{bst} = 380V$. The output power was swept using an electronic load, and the output voltage was recorded at a number of points, indicated with circles. The solid curves show predicted performance based on (7). While suitable for estimating a converter's peak power point, the model prediction is notably inadequate under more lightly loaded conditions. It is evident from Fig. 3 that the reactance model provides a computationally simple but qualitative approximation of the converter's power transfer capability.

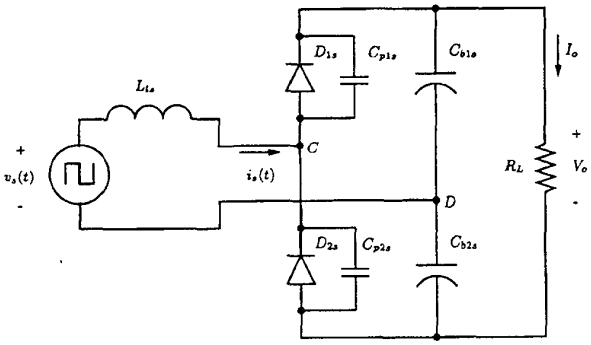

Fig. 4. Half-bridge rectifier with a capacitive filter.

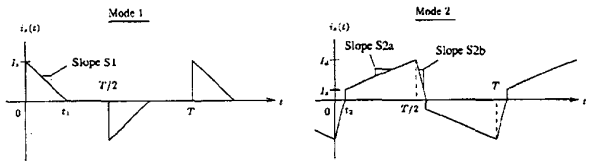

Fig. 5. Rectifier current modes.

IV. Switching Model

A more exact analytical prediction of the inverter transfer characteristic can be obtained using a switching model of the output rectifier in the DC-DC stage. This model will account for significant secondary effects that were previously ignored. In particular, the influence of the rectifier diodes during commutation is handled explicitly. Figure 4 shows the half-bridge rectifier using the previously discussed simplifications of the primary-side inverter and the transformer model. To simplify the current analysis, the diode depletion capacitances are assumed to be linear. The implications of this approximation will be discussed.

The secondary current $i_s(t)$ can be classified into one of two characteristic modes. The characteristic shapes for Modes 1 and 2 in steady-state operation are sketched in Figure 5. Although somewhat idealized, the shapes match well with the experimental data for the DC-DC stage for heavy and for light-load operation. In both modes the time average of the rectified secondary current is related to I_o:

$$\frac{<|i_s(t)|>}{2} = I_o. \tag{8}$$

A. Mode 1

Mode 1 occurs when the output is lightly loaded. Since $i_s(t)$ is odd harmonic (i.e., its positive and negative half-cycles are mirrors of each other), only the positive half-cycle needs to be described. The starting value of $i_s(t)$ at the beginning of each half-cycle is determined by a resonant ring of the secondary inductance and the diode parasitic capacitance at the moment of rectifier commutation. This is typically a fast ring and is modeled as a jump to a starting condition I_s in Fig. 5. Analysis of this resonant ring reveals that

$$I_s = \sqrt{\frac{2V_sV_oC_c}{L_{ls}}} \tag{9}$$

where $C_c = C_{p1s} + C_{p2s}$.

The current $i_s(t)$ then ramps quickly to zero so that the time-average relationship in (8) is maintained. The negative slope S_1 of $i_s(t)$ is determined by the voltage difference across the leakage inductance L_{ls}:

$$S_1 = (V_s - V_o/2)/L_{ls}. \tag{10}$$

For S_1 to be negative, V_o must be greater than V_s. Thus, the output voltage actually lifts instead of droops at light load. Given the starting value I_s and the slope S_1, the time average of $|i_s(t)|$ can be found from the average height of the Mode 1 waveform between $t = 0$ and $t = \frac{T}{2}$:

$$I_o = \frac{<|i_s(t)|>}{2} = -\frac{I_s^2}{2S_1T} = \frac{V_sV_oC_c}{(V_o/2 - V_s)T}. \tag{11}$$

This expression for I_o can be multiplied by V_o to produce an equation that relates the output power to the output voltage in Mode 1. By sweeping the value of V_o, (11) can be used to produce the desired plot of output voltage versus output power in Mode 1 or lightly-loaded operation. The rectifier will transition from Mode 1 to Mode 2 when S_1 becomes sufficiently shallow that $i_s(t)$ becomes continuous. From (10) and (11), the mode transition occurs when

$$I_o = \frac{I_s}{4} = \sqrt{\frac{V_sV_oC_c}{8L_{ls}}}. \tag{12}$$

B. Mode 2

In Mode 2 there are two distinct slopes, S_{2a} and S_{2b}.

$$S_{2a} = \frac{V_s - V_o/2}{L_{ls}} \qquad S_{2b} = \frac{-(V_s + V_o/2)}{L_{ls}} \tag{13}$$

The time t_2 is related to the slopes as follows:

$$t_2 = \frac{-(S_{2a}T/2 + I_s)}{S_{2b} - S_{2a}}. \tag{14}$$

The peak current I_d is given by,

$$I_d = -S_{2b}t_2. \tag{15}$$

Finally, the average mode 2 output current is

$$I_o = \frac{<|i_s(t)|>}{2} = \frac{I_s}{2}\left(\frac{1}{2} + \frac{S_{2a}T/2 + I_s}{T(S_{2b} - S_{2a})}\right) + \frac{I_dT}{4}. \tag{16}$$

By substituting for I_d and simplifying using the geometric relationships implied in Fig. 4,

$$I_o = \frac{4I_s^2 + 4I_sS_{2b}T + S_{2a}S_{2b}T^2}{8T(S_{2b} - S_{2a})}. \tag{17}$$

Substituting in expressions for the slopes S_{2a} and S_{2b} and the starting current I_s yields:

$$I_o = \frac{V_o^2T^2 + 32V_sV_oL_{ls}C_c - a(2V_s + V_o)T - 4V_s^2T^2}{-64TV_sL_{ls}}. \tag{18}$$

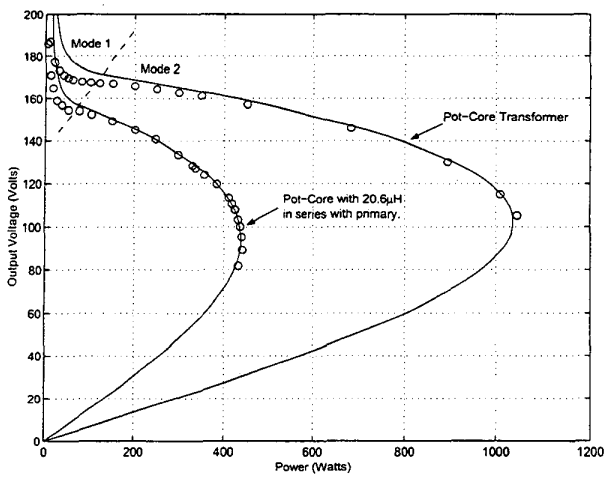

Fig. 6. Capability curve prediction using the switching model.

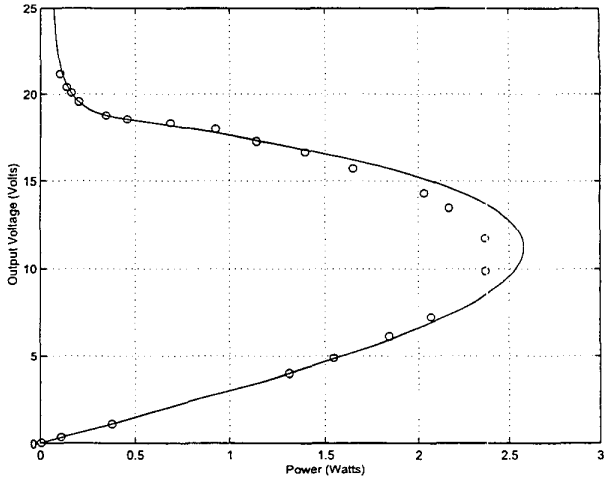

Fig. 7. Capability curve.

where

$$a = \sqrt{128 V_s V_o L_{ls} C_c}.$$

Again, this expression for I_o can be multiplied by V_o to produce an equation that relates the output power to the output voltage, in this case for Mode 2. By sweeping the value of V_o, (18) can be used to produce the desired plot of output voltage versus output power in Mode 2 operation.

V. Predicted and Measured Behavior

The results for Mode 1 and Mode 2 operation were spliced together in MATLAB® to generate an overall droop curve of V_o versus P_o. A sample "M-file" useful for generating these curves is contained within the Appendix. A typical result using parameters from the 1500 Watt experimental prototype is shown in Figure 6. Once again, the solid lines show the computer-aided prediction, while the circles indicating actual data measured from the prototype. Comparing Fig. 3 with Fig. 6 it is clear that the switching model offers a noticeable improvement over the reactance model, particularly during lightly loaded operations. There is still an apparent, increasing discrepancy that is seen for lighter and lighter loads. This discrepancy is largely the result of modelling the capacitances associated with the prototype rectifier diodes as linear. The linear capacitance approximation can significantly impact the accuracy of the Mode 1 calculation, because it directly affects the starting value of $i_s(t)$ at the start of each half-cycle.

Figure 7 shows a different set of predicted and measured capability curves for a DC-DC converter designed for use in an electromagnetic lock. The key and lock body contain the primary and secondary halves of a separable transformer, respectively. A total of about 3 watts of power is transferred across this inductive coupling during operation of the lock to provide power for the authentication electronics and locking mechanism in the lock body. The switches in this relatively low-power circuit are implemented with individual semiconductor devices. In the 1500 watt converter, the switches consisted of several paralleled devices to improve power handling capacity. It is relatively difficult to accurately characterize the nonlinear parasitics in the composite switches used in the larger converter. The individual devices in the smaller converter are easily characterized, and the predicted capability curve in Fig. 7 agrees well with measured data under light loading conditions. However, the transformer in the key and lock system provides very limited space for the primary and secondary windings, leading to a winding resistance to leakage inductance ratio higher than would be expected in a typical power transformer, e.g., the coupling used in the 1500 watt design. Because of the higher ohmic losses in the low power transformer, the idealized Mode 2 waveforms do not fully approximate those observed in the key and lock converter. Hence, the capability prediction in Fig. 7 shows some error near the peak loading conditions.

VI. Discussion

The resulting capability curves can be used to indicate whether or not a converter and coupling are capable of providing the needed operating point for a servomechanism. Figure 8, for example, illustrates a typical situation. The gray box indicates the design or capability specification for a converter intended to charge electrical vehicle batteries through an inductive coupling with the SAE-1773 practice. To charge a battery rack over a 30 percent voltage swing in a desired amount of time, the charger must be able to reach any point in the gray box. The capability curves show the performance of our completed design. Over an allowable range of input voltages from the boost converter, ranging from 267 to 390 volts, the charger and coupling are able to achieve any needed operating point in the design specification. Because these capability curves can be generated analytically using measured or estimated parameters from an inductive coupling, they are useful, among other applications, for evaluating candidate separable transformer designs for different servomechanical applications.

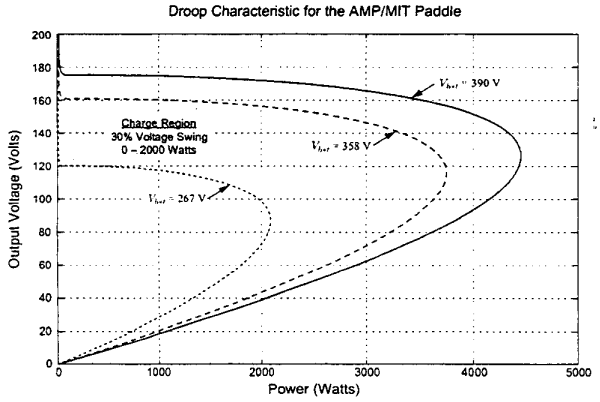

Fig. 8. Capability curve.

References

[1] D. Jackson, "Inductively Coupled Power Transfer for Electromechanical Systems," *Ph.D. Thesis*, Massachusetts Institute of Technology, May, 1998.

[2] K.W. Klontz, A. Esser, P.J. Wolfs, and D.M. Divan, "Converter Selection for Electric Vehicle Charger Systems with a High-Frequency High-Power Link," *Power Electronics Specialists Conference*, June, 1993, pp. 855-861.

[3] J.G. Bolger, C.A. Haslund, and R.J. Risser, "Inductive Charging of Electric Vehicles: Testing and Evaluation of an Automated System," *11th International Electric Vehicle Symposium*, September, 1992, pp. 1-12.

[4] D.M. Divan, K.W. Klontz, R.D. Lorenz, and D.W. Novotny, "Contactless Power Delivery System for Mining Applications," *IEEE Industry Applications Society Annual Meeting*, October, 1991, pp. 1263-1269.

[5] A. Esser, "Contactless Charging and Communication System for Electric Vehicles," *IEEE Industry Applications Society Annual Meeting*, October, 1993.

[6] A.W. Kelley and W.R. Owens, "Connectorless Power Supply for an Aircraft-Passenger Entertainment System," *IEEE Transactions on Power Electronics*, Vol. 4, No. 3, July 1989, pp. 348–354.

[7] A. Ghahary and B.H. Cho, "Design of a Transcutaneous Energy Transmission System Using a Series Resonant Converter," *IEEE Transactions on Power Electronics*, Vol. 7, No. 2, April 1992, pp. 261–269.

[8] D.J. Hind, "Inductively Coupled Battery Charging System," *Seventh Annual Battery Conference*, April, 1992.

[9] H. Mweene, "The Design of Front-End DC-DC Converters of Distributed Power Supply Systems with Improved Efficiency and Stability," *Ph.D. Thesis*, Massachusetts Institute of Technology, September, 1992.

[10] K.N. Bateson, "Class DE DC-DC Converters," *Proceedings of COMPEL 1998*, Cernobbio, Italy, pp. 119–125.

[11] J.G. Kassakian, M.F. Schlecht, and G.C. Verghese, *Principles of Power Electronics*, Addison-Wesley, 1991, pp. 395-399.

VII. Appendix

```
%%%%%%%%%%%%%%%%%%%%%%%%%%%%%%%%%%%%%%%%%%%%%%%%%%%%%%%%%%%%%%%%%%%%%%%%
% MATLAB Script: VDROOP.M                                                %
% ----------------------                                                 %
% This script calculates the voltage droop for a                         %
% Half-Bridge DC/DC converter using the Mode 1/2 model.                  %
%%%%%%%%%%%%%%%%%%%%%%%%%%%%%%%%%%%%%%%%%%%%%%%%%%%%%%%%%%%%%%%%%%%%%%%%

%%%%%%%%%%%%%%%%%%%%%%%%%%%%%%%%%%%%%%%%%%%%%%%%%%%%%%%%%%%%%%%%%%%%%%%%
%Measured or Estimated DC/DC converter parameters

Lp=16.0073e-6;          % Pri-side leakage inductance (T)
Ls=0.7812e-6;           % Sec-side leakage inductance (T)
Lm=174.5227e-6;         % Magnetizing inductance (T)
Np=25;                  % Primary turns
Ns=12;                  % Secondary turns
T=10e-6;                % Switching period
C=1200e-12;             % Diode capacitance, C=cp1s+cp2s
Vbst=380;          % Input bus voltage

%%%%%%%%%%%%%%%%%%%%%%%%%%%%%%%%%%%%%%%%%%%%%%%%%%%%%%%%%%%%%%%%%%%%%%%%
%Convert T-model to L-model and reflect across secondary

N=(Ns/Np);                      % Turns Ratio
Lls=N^2*(Ls+Lp*(Lm/(Lm+Lp))); %Sec-side leakage inductance
N2=N*(Lm/(Lm+Lp));              %L-model turns ratio
Vs=Vbst*N2/2;                   %reflected bus voltage

%%%%%%%%%%%%%%%%%%%%%%%%%%%%%%%%%%%%%%%%%%%%%%%%%%%%%%%%%%%%%%%%%%%%%%%%
%Initial Starting Current Calculation

Vo=[linspace(0,300,3000)];
Is=sqrt((2*Vs*Vo*C)/Lls);

%%%%%%%%%%%%%%%%%%%%%%%%%%%%%%%%%%%%%%%%%%%%%%%%%%%%%%%%%%%%%%%%%%%%%%%%
% Mode 1 calculation

S1=(Vs-Vo/2)/Lls;
Io1=-(Is.^2)./(2*S1*T);

%%%%%%%%%%%%%%%%%%%%%%%%%%%%%%%%%%%%%%%%%%%%%%%%%%%%%%%%%%%%%%%%%%%%%%%%
% Mode 2 calculation

S2a=(Vs-Vo/2)/Lls;
S2b=-(Vs+Vo/2)/Lls;
Io2=(4*Is.^2+4*Is.*S2b*T+S2a.*S2b*T^2)./(8*T*(S2b-S2a));

%%%%%%%%%%%%%%%%%%%%%%%%%%%%%%%%%%%%%%%%%%%%%%%%%%%%%%%%%%%%%%%%%%%%%%%%
% Calculate Power

P1a=Io1.*Vo;
P2a=Io2.*Vo;

%%%%%%%%%%%%%%%%%%%%%%%%%%%%%%%%%%%%%%%%%%%%%%%%%%%%%%%%%%%%%%%%%%%%%%%%
% Find the mode boundary and combine mode 1 & 2 results

trans=sum(Io2>Is/4);
cpa=[P2a(1:trans) P1a(trans+1:length(Vo))];

%%%%%%%%%%%%%%%%%%%%%%%%%%%%%%%%%%%%%%%%%%%%%%%%%%%%%%%%%%%%%%%%%%%%%%%%
% Plot voltage droop versus output power

figure(1)
plot(cpa,Vo,'-');
axis([0 1200 0 200]);
grid on
xlabel('Power (Watts)');
ylabel('Output Voltage (Volts)');
```